Korean Journal of Remote Sensing, Vol.23, No.1, 2007, pp.33~42

Speckle Removal of SAR Imagery Using a Point-Jacobian Iteration MAP Estimation

Sang-Hoon Lee †

Kyungwon University

Abstract : In this paper, an iterative MAP approach using a Bayesian model based on the lognormal distribution for image intensity and a GRF for image texture is proposed for despeckling the SAR images that are corrupted by multiplicative speckle noise. When the image intensity is logarithmically transformed, the speckle noise is approximately Gaussian additive noise, and it tends to a normal probability much faster than the intensity distribution. MRFs have been used to model spatially correlated and signal-dependent phenomena for SAR speckled images. The MRF is incorporated into digital image analysis by viewing pixel types as states of molecules in a lattice-like physical system defined on a GRF. Because of the MRF-GRF equivalence, the assignment of an energy function to the physical system determines its Gibbs measure, which is used to model molecular interactions.

The proposed Point-Jacobian Iterative MAP estimation method was first evaluated using simulation data generated by the Monte Carlo method. The methodology was then applied to data acquired by the ESA's ERS satellite on Nonsan area of Korean Peninsula. In the extensive experiments of this study, The proposed method demonstrated the capability to relax speckle noise and estimate noise-free intensity.

Key Words : SAR, Despeckling, Multiplicative Noise, Log-normal Distribution, MRF, Point-Jacobian Iteration.

1. Introduction

In the last couple of decades, the use of Synthetic Aperture Radar (SAR) has become increasingly popular because there are several well-known advantages of SAR data over other imaging systems (Leberl, 1990) including its capacity of imaging regardless weather conditions. However, the radar wave coherence produces "speckle" in SAR imagery. This phenomenon gives to the images a granular appearance that complicates image analysis and interpretation in remote sensing tasks. Although it is a deterministic phenomenon due to the coherent processing of terrain backscattering signals, the speckle contribution is often considered as noise that degrades the quality of SAR imagery. Speckle filtering is a common requirement in many SAR image applications. Up to now, speckle reduction remains a major issue in SAR imagery processing.

Speckle noise is supposed to be dependent on the

Received 2 January 2007; Accepted 21 February 2007.

† Corresponding Author: S. – H. Lee (shl@mail.kyungwon.ac.kr)

signal intensity in the sense that the noise level increases with the brightness. A simple statistical model based on multiplicative noise (Dainty, 1984) has been often used for the speckle reduction. Many adaptive filters have been developed to reduce multiplicative noise in SAR images by taking local statistics in order to distinguish between homogeneous regions and edges. The best-known filters include the Lee filter (Lee, 1986), Frost filter (Frost *et al.*, 1982), Kuan filter (Kuan *et al.*, 1985) and Gamma filter (Lopez *et al.*, 1993). The Frost filter was designed as an adaptive Wiener filter that assumed an autoregressive exponential model for the scene reflectivity. Kuan considered a multiplicative speckle model and designed a linear filter based on the minimum mean-square error criterion, optimal when both the scene and the detected intensities are Gaussian distributed. The Lee filter was a particular case of the Kuan filter based on a linear approximation made for the multiplicative noise model. The Gamma filter was based on a Bayesian analysis of the image statistics where both intensity and speckle noise follow a Gamma distribution.

If the number of scattering points per resolution cell is large, a fully developed speckle pattern can be modeled as the magnitude of a complex Gaussian field with independent and identically distributed real and imaginary components (Goodman, 1976). It leads to the Rayleigh distribution as the amplitude distribution model. Despite the theoretical appeal and the analytical simplicity of the Rayleigh model, high-resolution SAR images of urban scenes and some natural scenes such as sea surface deviate from the Rayleigh distribution (Anastassopoulos, 1999). Various models have been proposed to accommodate this problem. The Weibull distribution used in modeling urban scenes and sea clutter (Sekine and Mao, 1990), and the K-distribution successfully modeled sea clutter (Jao, 1984). Both are a special case of Rayleigh distribution. The lognormal models suggested for radar image intensity based on image statistics alone (Frankot and Chellappa, 1987).

Most SAR data are over-sampled by the SAR system to get pixel size less than the spatial resolution. Samples are then spatially correlated. Markov random fields (MRFs) (Kindermann and Snell, 1982) have been used to model spatially correlated and signal-dependent phenomena for SAR speckled images. Texture involves the spatial distribution of intensity in a local region. It contains important information about the structural arrangement of surfaces and their relationship to their neighboring surfaces. The MRFs represent a local interaction of image structure and have been demonstrated to be quite effective for texture characterization (Manjunath and Chellappa, 1990). The image textures have been represented with various statistical models of the MRF such a Gaussian MRF model (Walessa and Datcu, 2000), a casual Gaussian autoregressive random field model (Bouman and Liu , 1991), and a generalized Ising model (Andrey and Tarroux, 1998).

In this paper, an iterative *maximum a posteriori* (MAP) approach using a Bayesian model based on the lognormal distribution for image intensity and a Gibbs random field (GRF) for image texture is proposed for despeckling the SAR images that are corrupted by multiplicative speckle noise. When the image intensity is logarithmically transformed, the speckle noise is approximately Gaussian additive noise, and it tends to a normal probability much faster than the intensity distribution (Arsenault and April, 1976). The MRF is incorporated into digital image analysis by viewing pixel type s as states of molecules in a lattice-like physical system defined on a GRF (Georgii, 1979). Because of the MRF-GRF equivalence resulted from the Hammersley-Clifford theorem (Kindermann and Snell, 1982), the

assignment of an energy function to the physical system determines its Gibbs measure, which is used to model molecular interactions. The paper is organized as follows. Section 2 contains a description of the Bayesian model for the proposed speckle filter. The iterative MAP scheme and parameter estimation are presented in Sections 3 and 4 respectively. Experimental results of simulation data including comparison with those of the conventional techniques are reported and discussed in Section 5. Section 5 also contains the results of satellite SAR data acquired over an area of Korean Peninsula. Finally, conclusions are stated in Section 6.

2. Bayesian Function for MAP Estimation

The general model for SAR imagery is given by

$$z_k = v_k \eta_k + \varepsilon_k \tag{1}$$

where for the kth pixel, z_k and v_k are the noisy observation and noise-free intensity respectively, η_k and ε_k and are the corrupting multiplicative speckle noise and additive noise respectively. The despeckling problem is to restore the noise-free intensity.

Since the effect of additive noise in SAR images is generally much less significant than that of speckle noise, equation (1) can be rewritten as

$$z_k \cong v_k \eta_k. \tag{2}$$

The use of a logarithmic transform converts the multiplicative model into an additive one:

$$\ln z_k = \ln v_k + \ln \eta_k. \tag{3}$$

Let $I_n = \{1,2, \cdots, n\}$ be the set of indices of pixels in the image. If η_k follows a log-normal distribution, $\ln \eta_k$ follows a Gaussian distribution, and if $Y = \{y_k = \ln z_k, k \in I_n\}$, $X = \{x_k = \ln v_k, k \in I_n\}$, and σ_k^2 is a variance of $\ln \eta_k$, then

$Y \sim N(X, \Sigma)$ where $\Sigma = diagonal\{\sigma_k^2, k \in I_n\}$.

Image processes are assumed to combine the random fields associated with intensity and texture respectively. The objective measure for determining the optimal restoration of this "double compound stochastic" image process is based on Bayes' theorem. Given an observed image Y, the Bayesian method is to find the MAP estimate from the mode of the posterior probability distribution of the noise-free vector X, or equivalently, to maximize the log-likelihood function

$$lPN = \ln P(Y \mid X) + \ln P(X). \tag{4}$$

In the proposed algorithm, the MRF is used to quantify the spatial interaction probabilistically, that is, to provide a type of prior information on the image texture.

If R_i is the index set of neighbors of the ith pixel, $R = \{R_i \mid i \in I_n\}$ is a "neighborhood system" for I_n. A "clique" of $\{I_n, R\}$, c, is a subset of I_n such that every pair of distinct indices in c represents pixels which are mutual neighbors, and C denotes the set of all cliques. A GRF relative to the graph $\{I_n, R\}$ on X is defined as

$$\begin{aligned} P(X) &= Z^{-1} \exp\{-E(X)\} \\ E(X) &= \sum_{c \in C} V_c(X) \text{ (energy function)} \end{aligned} \tag{5}$$

where Z is a normalizing constant and V_c is a potential function which has the property that it depends only on X and c. Specification of C and V_c is sufficient to formulate a Gibbs measure for the region-class model. A particular class of GRF, in which the energy function is expressed in terms of non-symmetric "pair-potentials," is used in this study. The pair-potentials comprise a family of non-symmetric functions $\{V_p(i,j) \mid (i,j) \subset I_n\}$ satisfying $V_p(i,j) = 0$ if $i = j$ or $(i,j) \notin C_p$ where C_p is the pair-clique system (the term "non-symmetric" means that $V_p(i,j)$ is not equal to $V_p(j,i)$).

It is natural that neighboring pixels with more

similar intensity levels have a higher probability of having the same level. Based on this idea, spatial interaction can be quantified for image texture processes based on a distance measure between neighboring pixels. Here, the energy function of the GRF is specified as a quadratic function of X, which defines the probability structure of the texture process:

$$E_p(X) = \sum_{i \in I_n} \sum_{(i,j) \in C_p} \alpha_{ij}(x_i - x_j)^2 \quad (6)$$

where α_{ij} is a nonnegative coefficient vector which represents the "bonding strength" of the ith and the jth pixels.

The log-likelihood function of (4) using the log-normal intensity model and the GRF texture model is:

$$lPN \propto -(Y-X)'\Sigma^{-1}(Y-X) - X'\mathbf{B}X \quad (7)$$

where $\mathbf{B} = \{\beta_{ij}\}$ where

$$\beta_{ij} = \begin{cases} -\alpha_{ij} & \text{for } (i,j) \in C_p \\ \sum_{(i,j) \in C_p} \alpha_{ij} & \text{for } i = j \\ 0 & \text{otherwise} \end{cases} \quad (8)$$

is the bonding strength matrix.

3. Point-Jacobian Iteration MAP Estimation

Since the log-likelihood function of (7) is convex, the MAP estimate of X is obtained by taking the first derivative:

$$\Sigma^{-1}(Y-X) - \mathbf{B}X = 0. \quad (9)$$

The equation (9) can be solved by the point-Jacobian iteration (Varga, 1962). Decomposing the bonding strength matrix into a matrix with the diagonal elements and a matrix with the non-diagonal elements, the equation (9) is rewritten as

$$\begin{aligned} &X = \mathbf{M}_d^{-1}\Sigma^{-1}Y - \mathbf{M}_d^{-1}\mathbf{B}_s X \\ &\mathbf{M}_d = diagonal\{\sigma_k^{-2} + \beta_{kk}, k \in I_n\}. \\ &\mathbf{B}_s = \{\beta_{ij} \mid \text{diagonal elements are zeros}\} \end{aligned} \quad (10)$$

The noise-free intensity can be recovered iteratively: given an initial estimate of $X, \hat{X}^0$ at hth iteration

$$\hat{X}^h = \mathbf{M}_d^{-1}\Sigma^{-1}Y - \mathbf{M}_d^{-1}\mathbf{B}_s\hat{X}^{h-1}, \quad (11)$$

equivalently

$$\hat{x}_i^h = \frac{1}{\sigma_i^{-2} + \beta_{ii}}\left[\sigma_i^{-2} y_i - \sum_{(i,j) \in C_p} \beta_{ij}\hat{x}_j^{h-1}\right], \ \forall i \in I_n. \quad (12)$$

The iteration converges to a unique solution since $\gamma(\mathbf{M}_d^{-1}\mathbf{B}_s) < 1$ where $\gamma(\cdot)$ denotes the spectral radius (Cullen, 1972).

4. Bonding Strength Coefficient Estimation

Various regions constituting an image can be characterized by textural components. The bonding strength coefficients of (6) are associated with local interaction between neighboring pixels and can provide some contextual information on the local region. It is important to choose the coefficients suitable for the analyzed image. Given a constant r, the Bayesian MAP estimation of (7) can be considered as an optimization problem:

$$\begin{aligned} &\arg\min_X \left\{ \sum_{i \in I_n} \sum_{(i,j) \in C_p} \alpha_{ij}(x_i - x_j)^2) \right\} \text{ subject to} \\ &\sigma_k^{-2}(y_k - x_k)^2 < r, \ \forall k \in I_n. \end{aligned} \quad (13)$$

Since the objective function and the constraints are convex, the optimization of (13) is restated as

$$\arg\min_X \left\{ \sum_{i \in I_n} \left[\sum_{(i,j) \in C_p} \alpha_{ij}(x_i - x_j)^2 + \lambda_i\left(\sigma_i^{-2}(y_i - x_i)^2 - r\right) \right] \right\}, \quad (14)$$

where λ is a "Lagrangian coefficient." By taking $\{\alpha'_{ij} = \alpha_{ij} / \lambda_i\}$ instead of $\{\alpha_{ij}\}$, the problem of (14) is equivalent to the maximization of the log-likelihood function of (7). Suppose $\{\alpha_{ij}, j \in I_n \mid \sum_{j \in I_n} \alpha_{ij} = 1\}$ as the normalized coefficients associated with the relative strength of interaction between the individual types of pair-cliques at the ith pixel. These interaction coefficients represent a textural component for the local

region corresponding to the ith pixel, and, adopting a Bayesian interpretation, $\phi_i = 1/\lambda_i$ is referred to as a parameter that represents the relative strength of prior beliefs compared to information on the observation.

If the normalized interaction coefficients are predetermined, the parameters $\{\phi_i\}$ are then estimated from:

$$\begin{aligned} &\Sigma^{-1}(Y-X) - \mathbf{PB}X = 0 \\ &\sigma_k^{-2}(y_k - x_k)^2 < r, \ \forall k \in I_n \end{aligned} \quad . \tag{15}$$

where $\mathbf{P} = diagonal\{\phi_k, k \in I_n\}$, and for $\gamma(\Sigma\mathbf{PB}) << 1$,

$$\hat{X} = (\mathbf{I} + \Sigma\mathbf{PB})^{-1} Y \approx (\mathbf{I} - \Sigma\mathbf{PB})Y. \tag{16}$$

Then,

$$\hat{\phi}_i = \sqrt{\frac{r}{\sigma^2 \sum_{(i,j)\in C_p} \alpha_{ij}(y_i - y_j)^2}}, \forall i \in I_n. \tag{17}$$

As mentioned in Section 3, it is natural that neighboring pixels with more similar intensity levels have a higher probability of having the same level. Under this supposition, the normalized coefficients can be chosen as

$$\hat{\alpha}_{ik} = \begin{cases} \dfrac{(y_i - y_k)^{-2}}{\sum_{(i,j)\in C_p} (y_i - y_j)^{-2}} & \text{for } (i,k) \in C_p. \\ 0 & \text{otherwise} \end{cases} \tag{18}$$

The estimate of X in (16) approximates the optimal solution as a weighted sum of the values of the center and neighboring pixels, and thereby the parameters $\{\phi_i\}$ are determined reasonably from (16), even for the cases not satisfying $\gamma(\Sigma\mathbf{PB}) << 1$. The constant r is a parameter related to the distribution of Y and its appropriate choice is unit value.

5. Experiments

The proposed Point-Jacobian Iterative MAP (PJIMAP) estimation method was first evaluated using simulation data generated by the Monte Carlo method. The methodology was then applied to data acquired by the ESA's ERS satellite on Nonsan area of Korean Peninsula.

For the experimenst, 16-bit simulation images of multiplicative noise model were generated using various patterns. The 4 image patterns used in this section are illustrated in Fig. 1. In this study, the neighborhood system used a square window, for example, in the first order system, the 8 pair-clique types are defined on 3×3 window: for the (i,j)th pixel, they are $[(i,j),(i,j+1)]$, $[(i,j),(i,j-1)]$, $[(i,j),(i+1,j)]$, $[(i,j),(i-1,j)]$, $[(i,j),(i+1,j+1)]$, $[(i,j),(i-1,j+1)]$, $[(i,j),(i+1,j-1)]$, $[(i,j),(i-1,j-1)]$ (note that the pixel index used in the previous sections is one-dimensional expression, while the index in this section is 2-D expression). The variance σ_{ij}^2 was estimated using the average value of observed intensities in the neighbor-window:

$$\hat{\sigma}_{ij}^2 = \frac{(x_{ij} - \hat{\mu}_{ij})^2}{n_w} \text{ and } \hat{\mu}_{ij} = \frac{\sum_{ij\in W_{ij}} x_{ij}}{n_w} \tag{19}$$

where n_w is the number of pixels in the neighbor-

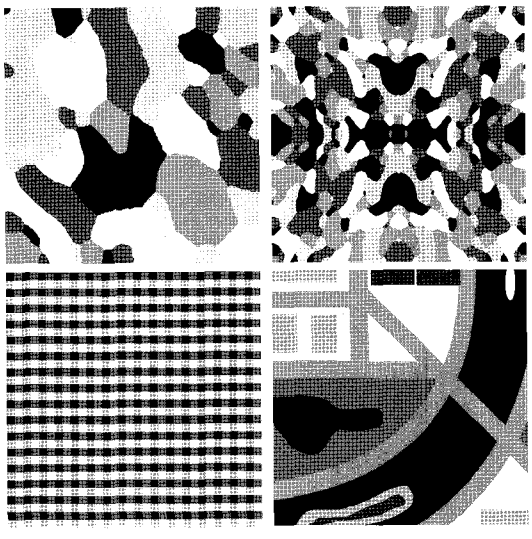

Fig. 1. Image patterns for simulation: clockwise from north-west corner - A, B (5classes), E (4classes), F (7 classes).

window and W_{ij} is the set of indices belonging to the window of the (i,j)th pixel. It is difficult to find a correct textural component in the noisy observation. The bonding strength coefficients were estimated using $\{\hat{\mu}_{ij}\}$ instead of the observed values $\{y_{ij}\}$, and the initial estimates $\{\hat{x}_{ij}^0\}$ were chosen as $\{\hat{\mu}_{ij}\}$. A threshold for the condition of convergence in (12) is defined as

$$k\sqrt{\frac{\sum_{\forall_{ij}}\hat{\sigma}_{ij}^2}{n}} \qquad (20)$$

where $k<<1$ is a given constant. In the simulation experiments, k was given with 0.001.

First the speckle filters were applied to the simulation data of pattern A. The simulated noisy observation image and the histogram of intensity values are shown in the first row of Fig. 1. Pattern A has 5 classes and with the noise-free intensities of 500, 1000, 1500, 2000, 2500. The number of pixels belonging to each class is displayed by the bar graph in Fig. 1. The observations are ranged in 0 and 12070 with a left-skew distribution. In the second and third

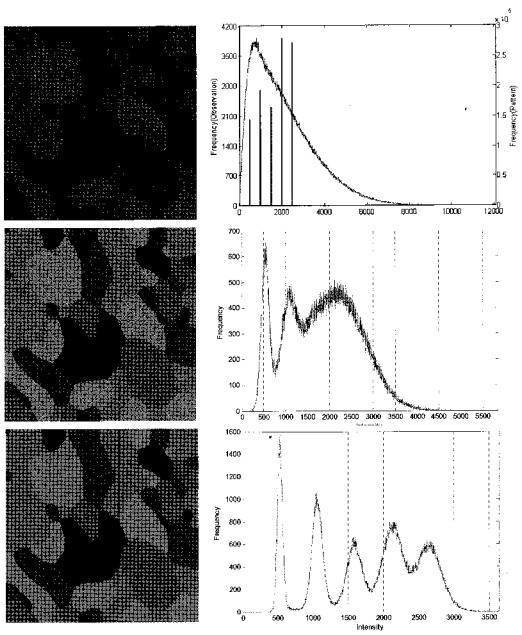

Fig. 2. Results of PJIMAP despeckling and histograms: from top, observed image, despeckled image of 1st order neighborhood, despeckled image of 3rd order neighborhood (the bar graph in the first histogram displays the pixel number of each class).

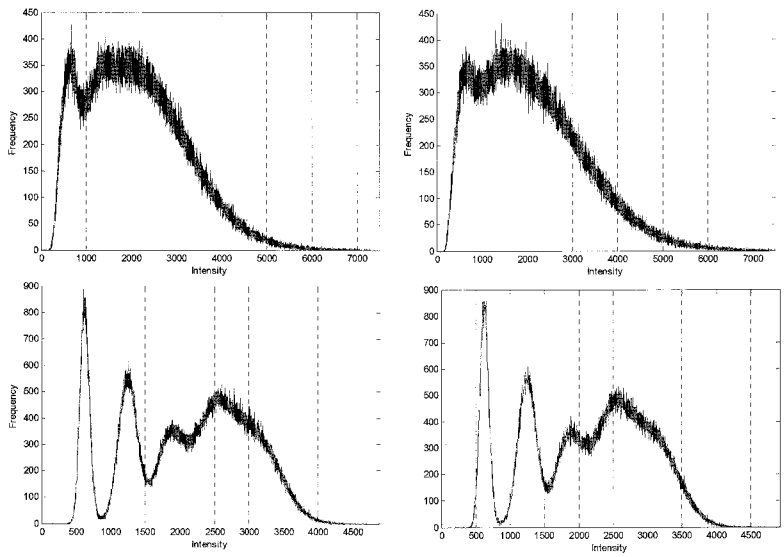

Fig. 3. Histogram results of conventional speckle filters using 5×5 window for simulation data in Fig. 2: clockwise from north-west corner - Kuan, Lee, Frost*, Gamma (*Frost has 8176 pixels of zero values).

Table 1. Statistics of despeckled results of simulation data of pattern A.

Filter	Minimum	Maximum	Sample Mean	Sample Standard Deviation
noise-free data	500	2500	1663.4	693.2
noisy data	1	12070	2084.6	1465.9
PJIMAP-1	162	5846	1797.3	826.3
PJIMAP-3	368	3640	1761.2	739.2
Kuan	0	53466	2085.2	1099.2
Lee	128	9667	2084.3	1158.6
Frost	0	4883	2066.3	909.6
Gamma	110	4918	2084.8	890.4

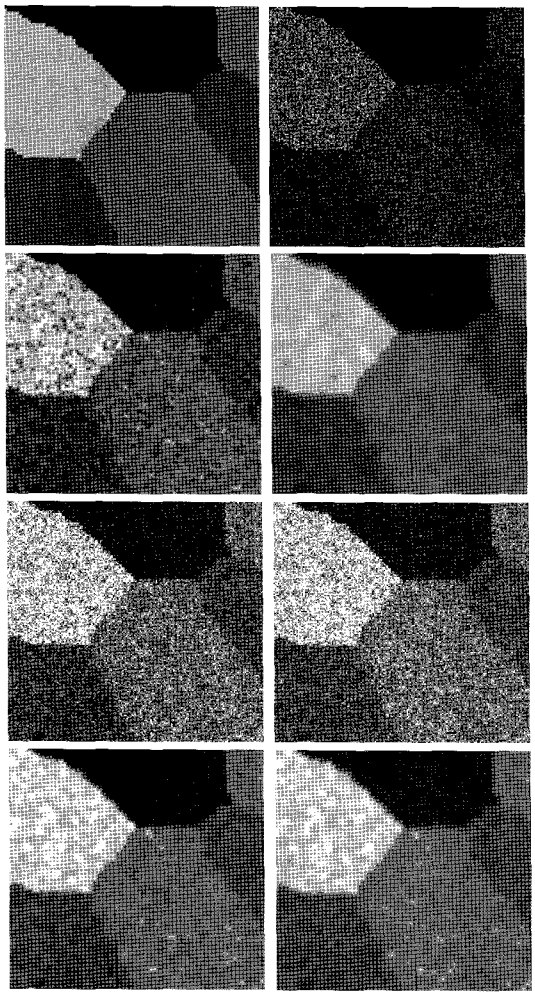

Fig. 4. Sub-areas of despeckled images using six speckle filters: from top, noise-free and observed noisy images (1st row), PJIMAP-1 and PJIMAP-3 (2nd row), Kuan and Lee (3rd row), Frost and Gamma (4th row).

rows, the results of despeckling using the PJIMAs of the first order (PJIMAP-1: 3×3 neighborhood window) and third order (PJIMAP-3: 5×5 neighborhood window) are illustrated. As shown in the figure, the result of PJIMA-3 quite well agrees with the true pattern, while PJIMAP-1 more or less failed in relaxing speckle noise for higher intensity values. The same data were also despeckled by the most notorious adaptive filters using 5×5 window. The histogram results are contained in Fig. 3. The Kuan and Lee filters yielded similar results, but the distribution of their results still lean to the left. The Frost and Gamma filters show better performance than the other adaptive filters, but they are not successful in fitting on the pattern. The summits of their histograms are deviated from the points corresponding to the true pattern and the resultant intensities still remain in the higher range compared to the PJIMAPs'. It shows in Table 1 that contains the statistics of despeckled results. As shown in the table, the PJIMAPs produced the results harmonizing with the true pattern. In case of the Frost's, it generated a considerable number of zeros (8176 pixels have zero estimates). The Kuan and Lee filters generated some very high values. Fig. 4 displays the detailed images of sub-area for the despeckled data It also shows that PJIMAP-3 yielded the result close to the noise-free intensity image. The results of the Kuan and Lee filters still have significant grainy pattern, and the others seems to require more relaxation. Next the simulation study was extended for different patterns. Figs. 5, 6 and 7 contain the results of the PJIMAP-3 and Gamma filters. They indicate that evaluation on the performance of the filters are similar to the case of simulation data of pattern A.

In this experiment, the speckle filters were applied to the SAR image remotely-sensed by the ESA's ERS satellite. This data was acquired over Nonsan area on Korean Peninsula in the summer of 2004.

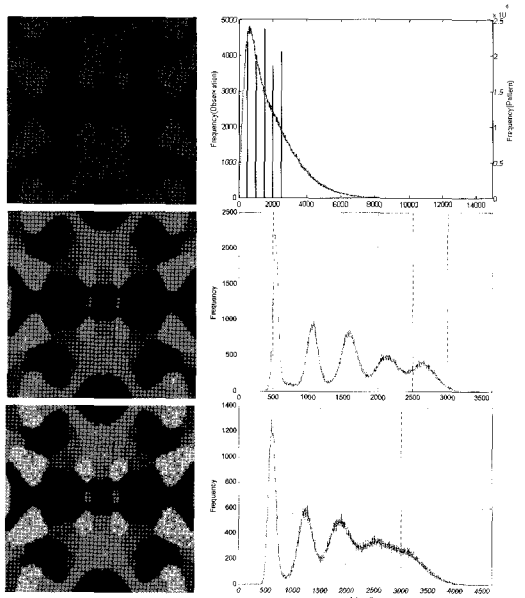

Fig. 5. Results of PJIMAP and Gamma despeckling and histograms: from top, noise-free and observed noisy images (1st row), PJIMAP-3 (2nd row), Gamma of 5×5 window (3rd row).

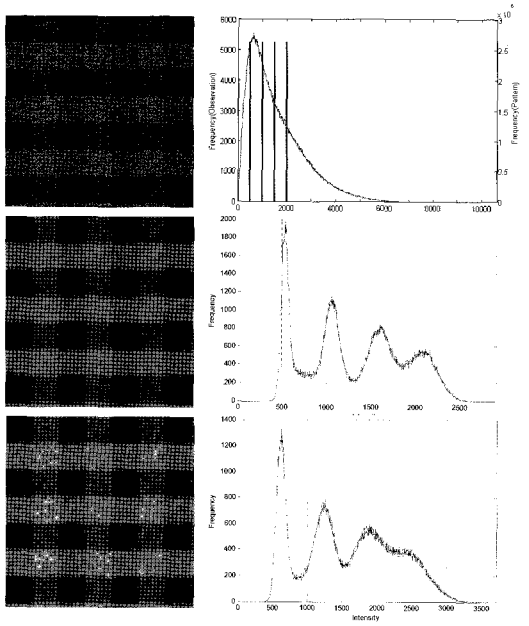

Fig. 6. Results of PJIMAP and Gamma despeckling and histograms: from top, noise-free and observed noisy images (1st row), PJIMAP-3 (2nd row), Gamma of 5×5 window (3rd row).

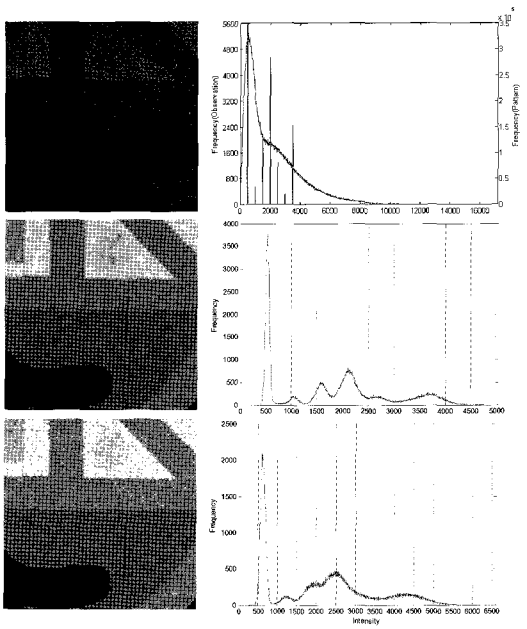

Fig. 7. Results of PJIMAP and Gamma despeckling and histograms: from top, noise-free and observed noisy images (1st row), PJIMAP-3 (2nd row), Gamma of 5×5 window (3rd row).

Fig. 8 displays the images despeckled by PJIMAP-1, PJIMAP-3, and Gamma filter. The result of PJIMAP-3 is too much smoothed and it failed in preserving the

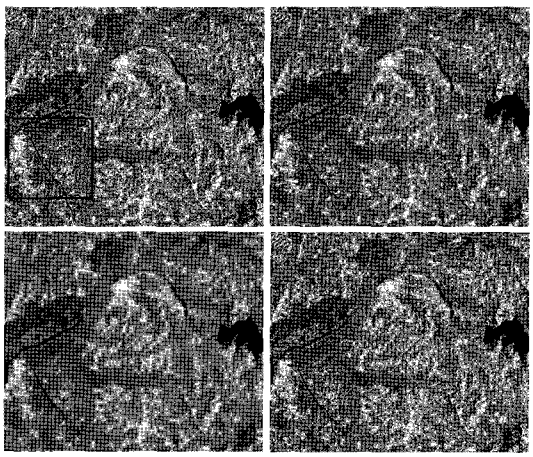

Fig. 8. Results of despeckling ESA's ERS Satellite SAR image acquired over Nonsan area in Korean Peninsula: clockwise from north-west corner - Observed image,despeckled images by PJIMAP-1, PJIMAP-3, and Gamma of 3×3 window.

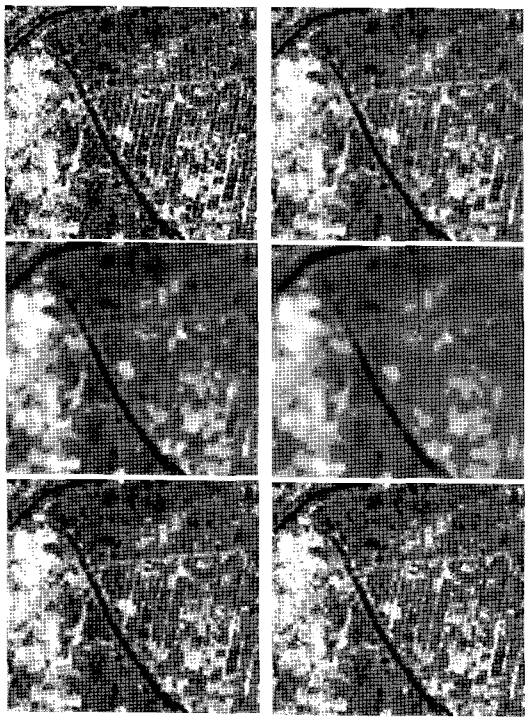

Fig. 9. Results of squared area in Fig. 8 using 5 speckle filters: from top, observed images and PJIMAP-1 (1st row), PJIMAP-2 and PJIMAP-3 (2nd row), PJIMAP-1* and Gamma (3rd row) (* more strict convergence threshold).

detailed structure, and the speckle noise of higher values remains in the result of Gamma filter. In the result image of PJIMAP-1, the speckle noise is reasonably relaxed and the detailed structure exhibited in the observation is maintained. Fig. 9 displays the sub-images of the squared area in the observed image of Fig. 8. The observation shows that the scene of the sensed area has a complicated textural component with small and narrow feature. Due to this fact, the larger order systems of PJIMAP do not work well to correctly analyze the data. The Gamma filter are successful in keeping the structure, but failed in removing the speckle noise in the area of high intensity, and even generated some distorted estimates. The close look confirms that PJIMAP-1 yielded a robust estimation of this real SAR data. In Fig. 9, two results of PJIMAP are illustrated. One is the result with k = 0.001 and the other with k = 0.0001. These are very similar. More iteration is plausible to generate more reliable estimation in detailed values, however.

6. Conclusions

PJIMAP filter is proposed for despeckling SAR imagery, which is an iterative approach to find MAP estimation of noise-free intensity. In the extensive experiments of this study, PJIMAP demonstrated the capability to relax speckle noise and estimate noise-free intensity. The algorithm is established based on a multiplicative noise model using a log-normal distribution and a texture model using GRF. The log-normal distribution provides a convenient means to analyze the data with use of a multiplicative model. There exists an argument that the log-normal distribution fails in modeling the lower half of the SAR histograms (Kuttikkad and Chellappa, 1994). However, the simulation study indicates that despeckling has more problems in the range of higher values. The GRF is used to probabilistically quantify spatial interaction between neighbor pixels to represent a textural component of the image structure. It is important to choose an appropriate neighborhood system defining the GRF. A larger order of neighborhood system smoothes the image to some extent, and it results in results in fading the detailed features existed in the scene.

References

Anastassopoulos, V., G. A. Lampropoulos, and M. Rey, 1999. High resolution radar clutter statistics. *IEEE Trans. Aerosp. Electron. Syst.*, 35: 43-60.

Andrey P. and P. Tarroux, 1998. Unsupervised segmentation of Markov random field modeled textured images using selectionist relaxation. *IEEE Trans. Pattern Anal. Mach. Intell.*, 20: 252-262.

Arsenault H. H. and G. April, 1976. Properties of speckle integrated with a finite aperture and logarithmically transformed. *J. Opt. Soc. Amer.*, 66: 1160-1163.

Bouman C. and B. Liu, 1991. Multiple resolution segmentation of textured images. *IEEE Trans. Pattern Anal. Mach. Intell.*, 13: 99-113.

Chellappa, R. and S. Chatterjee, 1985. Classification of textures using Gaussian Markov random fields. *IEEE Trans. Acoustics,Speech, and Signal Proc.*, 33: 959-963.

Cullen, C. G., 1972. *Matrices and Linear Transformations.* Reading, MA: Addison-Wesley.

Dainty, J. C., 1984. *Laser Speckle and Related Phenomena*, Second Enlarged Edition.

Frankot, R. T. and R. Chellapa, 1987. Lognormal random-field models and their applications to radar image synthesis. *IEEE Trans. Geosci. Remote Sens.*, 25: 195-207.

Frost, V. S., J. A. Stiles, K. S. Shanmugan, and J. C. Holtzman, 1982. A model for radar images and its application to adaptive digital filtering of multiplicative noise. *IEEE Trans. Pattern Anal. Mach. Intell.*, 4: 157-165

Georgii, H. O., 1979. *Canonical Gibbs Measure.* Berlin, Germany: Springer-Verlag.

Goodman, J. W., 1976. Some fundamental properties of speckle. *J. Opt. Soc. Amer.*, 66: 1145-1150.

Jao, J. K., 1984. Amplitude distribution of composite terrain clutter and the k-distribution. *IEEE Trans. Antennas Propagat.*, 32: 1049-1062.

Kuan, D. T., A. A. Sawchuk, and P. Chavel, 1985. Adaptive noise smoothing filter for images with signal-dependent noise. *IEEE Trans. Pattern Anal. Machine Intell.*, 7: 165-177.

Kindermann R. and J. L. Snell, 1982. *Markov Random Fields and Their Application*, Providence, R. I.: Amer. Math. Soc.

Kuttikkad S. and R. Chellappa, 1994. Non-Gaussian CFAR techniques for target detection in high resolution SAR images, *Proc. ICIP-94*, pp. 910-914.

Leberl, F., 1990. *Radargrammetric image processing*, Artech House, Inc.

Lee, J. S., 1986. Speckle suppression and analysis for synthetic aperture radar. *Optical Engineering*, 25: 656-643.

Lopes, A., E. Nezry, R. Touzi, and H. Laur, 1993. Structure detection and statistical adaptive speckle in SAR images. *International Journal of Remote Sensing*, 13: 1735-1758.

Manjunath, B. S. and R. Chellappa, 1991. Unsupervised texture segmentation using Markov random field models. *IEEE Trans. Patt. Anal. Mach. Int.*, 13: 478-482.

Sekine, M. and Y. Mao, 1990. *Weibull Radar Clutter*, London, U.K.: IEE Press.

Ulaby, F. T. and M. Craig Dobson, 1989. *Handbook of radar scattering statistics for terrain*, Norwood, MA : Artech House.

Varga, R. S., 1962. *Matrix Iterative Analysis*, Englewood Cliffs, NJ: Prentice-Hall.

Walessa M.and M. Datcu, 2000. Model-based despeckling and information extraction form SAR images. *IEEE Trans. Geosci. Remote Sens.*, 38: 2258-2269.